Robust Design Approaches for Hybrid Rocket Upper Stage

Robust Design Approaches for Hybrid Rocket Upper Stage

L. Casalino[1], F. Masseni[2], and D. Pastrone[3]

[1]Professor, PhD., Politecnico di Torino, Dipartimento di Ingegneria Meccanica e Aerospaziale, Corso Duca degli Abruzzi, 24.

[2]PhD. Candidate, MSc., Politecnico di Torino, Dipartimento di Ingegneria Meccanica e Aerospaziale, Corso Duca degli Abruzzi, 24. Email: filippo.masseni@polito.it

[3]Professor, MSc., Politecnico di Torino, Dipartimento di Ingegneria Meccanica e Aerospaziale, Corso Duca degli Abruzzi, 24.

ABSTRACT

Computational cost of robust-based design optimization methods may be very high. Evaluation of new procedures for the management of uncertainty with application to hybrid rocket engines is here carried out. Two newly developed procedures are presented (hybrid algorithm and iterated local search) and their performance are compared to those of two previously developed procedures (genetic algorithm and particle swarm optimization). A liquid-oxygen/paraffin-based fuel hybrid rocket engine which powers the third stage of a Vega-like launcher is considered. The conditions at third-stage ignition are assigned and a proper set of parameters are used to define the engine design and compute the payload mass. Uncertainties in the regression rate are taken into account. An indirect trajectory optimization approach is used to determine a mission specific objective function, which takes into account both the payload mass and the ability of the rocket to reach the required final orbit despite uncertainties. Results show that, for this kind of problems, particle swarm optimization and iterated local search outperform the genetic algorithm, but the use of a local search operator may slightly improve its performance.

INTRODUCTION

Hybrid Rocket Engines (HREs) gather many positive features from both Liquid Rocket Engines

(LREs) and Solid Rocket Motors (SRMs). HREs performance are close to semi-cryo or storable LREs while they are cheaper than SRMs. HREs are also safer and more environmentally friendly than both LREs and SRMs. Thus, the development of HREs is the focus of a great number of research programs worldwide. A large number of applications are being studied, including micro gravity platforms, hypersonic accelerators, small satellites, upper stage for small launchers, launchers from Mars, Moon landers, debris removals and commercial space flights (Casalino and Pastrone 2008; Jens et al. 2016; Dornheim 2004; Casalino and Pastrone 2012; Karp et al. 2016). In HREs only one propellant (i.e. the liquid one) flow can be controlled. Therefore, only one of thrust and mixture ratio can be freely set. This typical behavior requires a proper multidisciplinary design optimization approach, which should include a coupled optimization of the propulsion system and trajectory. Moreover, uncertainties may cause severe deviation of the performance from the nominal one, so that the expected mission could be not accomplished. For example, regression rate plays a role in the design and operation in HREs (Pastrone 2012), and even small uncertainty in its determination may jeopardize vehicle performance and threaten seriously the mission (Casalino and Pastrone 2015). In order to reduce the sensitivity of the engine performance to uncertainties, a robust-based design approach can be used. Different definitions of robust design can be found in literature (Taguchi et al. 2000; Suh 2001; Box and Fung 1993), but, anyway, they generally share a common background. In the present article the basic concept of ”robustness” can be summarized as ”the capability of the system to grant a fixed level of performance” (i.e. to match mission goals), ”minimizing the effect of uncertainties in the design parameters without eliminating their causes” (Taguchi et al. 2000; Park et al. 2006). Robust-based design optimization may be a very demanding task, since the computational cost grows exponentially with the number of uncertain quantities taken into account. Then, the selection of fast and reliable procedures is, not only strongly advisable but, in most cases, necessary. Two new robust-based design procedures are here proposed and compared to two other available algorithms, namely a Genetic Algorithm (GA) and a Particle Swarm Optimization (PSO). The purpose is to develop and compare algorithms based on different principles, aiming at the reduction of the computational effort. In the first new procedure,

called Hybrid Algorithm (HA), the performance of GA is enhanced by means of a local search operator. The second new proposed procedure is an Iterated Local Search algorithm (ILS). Both of these procedures exploit Taguchi's robust design approach. The design of an upper stage is here considered. Previous studies highlighted that HREs are a viable option for small and/or low-cost launchers and they can grant a very good margin of payload improvement (Casalino et al. 2014). Different propellant combinations were considered for the case study of a hybrid rocket engine upper stage suitable for the replacement of Vega launcher third and fourth stages (Isakowitz et al. 2004) and a deterministic optimization was carried out. The optimization aim was the maximization of the payload inserted into a reference orbit. In subsequent studies, a robust design optimization was performed considering one propellant combination, i.e. hydrogen-peroxide/ polyethylene; throat erosion was neglected to simplify the problem. Results showed that robustness in the design could be achieved with a small payload reduction which is necessary to ensure mission goals matching (Casalino and Pastrone 2016). For the present work the same application is considered, adopting a Liquid OXygen (LOX)/wax propellant combination due to its promising performance (Cantwell et al. 2010). Only uncertainties on the classical regression rate correlation are taken into account. Nozzle throat erosion is regarded from a deterministic point of view (uncertainties in erosion parameters are here neglected). A combined procedure is used (Casalino and Pastrone 2005a): an indirect method optimizes the trajectory for each combination of engine parameters (Casalino et al. 1999; Casalino and Pastrone 2005b; Casalino and Pastrone 2013) which, in turn, are selected by a proper robust optimization method. In all optimization runs, the objective function is evaluated as a linear combination of payload (that is not affected by uncertainty) and an index that quantifies the effective reaching of the target orbit, based on the average performance under uncertainty. Many optimization runs are carried out at fixed computational cost (in terms of number of objective function evaluations N_{FE}, equal to 4000, i.e. $N_{FE,max} = 4000$). In the following sections, first of all the authors sum up the main features of grain geometry, ballistic model and indirect optimization procedure. Then they describe the algorithms used in the robust optimization of engine model parameters. Finally, the authors compare numerical results of the different optimization methods

used, making our conclusions.

NUMERICAL MODELS

Grain Geometry and Ballistic Model

LOX/wax is here considered as propellant combination for HREs design. Cryogenic LOX is stored in liquid phase in a tank and injected into the combustion chamber during operation. Wax is stored in solid phase as a cylindrical grain in the combustion chamber. Paraffin-based fuels, such as wax, present an unstable melt liquid layer that causes the entrainment of droplets into the gas stream (Karabeyoglu et al. 2002). This mechanism strongly increases the fuel mass transfer rate into the flame zone where combustion takes place through diffusive mixing of oxidizer and fuel coming from the grain. For this reason, regression rate is relatively large and a single circular port can be adopted for the fuel grain while classical fuels would require a multi-port grain design to avoid excessive length to diameter ratio, L/D (Casalino and Pastrone 2016). The geometry of the circular-port grain is defined by the grain outer radius R_g, the web thickness w, and the grain length L_b. The initial inner radius, i.e. the port radius before ignition, results to be $R_i = R_g - w$. For any given burning distance y ($0 \leq y \leq w$) the burning perimeter P and the port area A_p can be evaluated:

$$P = 2\pi (R_i + y) \tag{1}$$

$$A_p = \pi (R_i + y)^2 \tag{2}$$

The authors use an approximate relation between chamber head-end pressure p_1 and chamber nozzle-stagnation pressure p_c to take into account pressure losses inside the combustion chamber (Barrere et al. 1960):

$$p_1 = \left[1 + 0.2 \left(\frac{A_{th}}{A_p} \right)^2 \right] p_c \tag{3}$$

where A_{th} is the throat area. The regression rate is assumed to be uniform along the port axis and the combustion of the lateral end is neglected. Its value is determined by the oxidizer mass flow

rate $\dot{m}_O$ and grain geometry:

$$\dot{y} = a\,(\dot{m}_O/A_p)^n \tag{4}$$

In the present work a and n are assumed to be uncertain parameters. Their reference nominal values are $a = 9.1 \cdot 10^{-5}\,\mathrm{m^{2n+1}s^{n-1}kg^{-n}}$ and $n = 0.69$ when the International System of Units is used (Karabeyoglu et al. 2002). The hydraulic resistance Z in the oxidizer flow path from the tank to the combustion chamber determines the oxidizer flow rate. Under the assumption of incompressible turbulent flow:

$$\dot{m}_O = \sqrt{(p_t - p_1)/Z} \tag{5}$$

where p_t is the oxidizer tank pressure. The authors assume a constant value of Z during the operation. One can obtain fuel mass flow $\dot{m}_F$ as:

$$\dot{m}_F = \rho_F \dot{y} A_b = \rho_F \dot{y} L_b P \tag{6}$$

where ρ_F is the fuel grain density, A_b is the burning area. The relative contribution of lateral end to combustion at the beginning of the burn $\left(\frac{A_{le}}{A_b}\right)_{\%}$ can be computed by means of Eq. (7) and will be checked "a posteriori" for optimal solutions.

$$\left(\frac{A_{le}}{A_b}\right)_{\%} = \frac{(R_i + R_g)w}{2R_i L_b} \cdot 100 \tag{7}$$

The mixture ratio α can be computed as:

$$\alpha = \frac{\dot{m}_O}{\dot{m}_F} \propto \dot{m}_O^{1-n} A_p^n / A_b \tag{8}$$

An isentropic expansion in the nozzle is assumed, and the chamber nozzle-stagnation pressure p_c is determined by:

$$p_c = \frac{(\dot{m}_O + \dot{m}_F)c^*}{A_{th}} \tag{9}$$

A chamber pressure of 10^6 Pa is used in performance evaluation of the propellant combination as a function of the mixture ratio α. Even though the actual pressure in the combustion chamber can span over a wide range during engine operations, the error is small for chamber pressures and mixture ratios considered in this article. The authors assume frozen equilibrium expansion: exhaust gas composition is kept constant throughout the nozzle and equal to combustion chamber one. The conservative assumption of frozen equilibrium expansion is adopted to account for the low combustion efficiency of HREs. Moreover a $0.96c^*$-efficiency (Sutton and Biblarz 2001) is introduced. In order to compute accurately and quickly the proper values as the mixture ratio changes during operation, the authors embed in the code third-degree polynomial curves, fitting the characteristic velocity and specific heat ratio, in the code (Mc Bride et al. 1994). A partially regulated feed system is considered with two operational modes: a first phase with constant tank pressure, maintained by means of helium flowing from an auxiliary tank, and a second Blow-Down (BD) phase.

The initial ullage volume $\left(V_g\right)_i$ is assumed to be 3% of the oxidizer volume. In this way one can obtain a stable regulator response when the out flow starts (Brown 1992). Two additional parameters are needed: the auxiliary gas tank volume V_a and the initial pressurizing gas pressure p_a. The first is conveniently replaced by the exhausted oxidizer mass at the beginning of the BD phase $(m_O)_{BD}$ and the latter is fixed at $p_a = 2.00 \cdot 10^7$ Pa (Casalino and Pastrone 2010). During the first operational mode $p_t = (p_t)_i$ whereas during the BD phase p_t is calculated assuming an isentropic expansion of the pressurizing gas in the oxidizer tank:

$$p_t = (p_t)_i \left[\frac{(V_g)_{BD}}{V_g} \right]^{\gamma_g} \tag{10}$$

where the gas volume in the tank $V_g = \left(V_g\right)_i + m_O/\rho_O$ depends on the oxidizer mass m_O that has been exhausted, $\left(V_g\right)_{BD} = \left(V_g\right)_i + (m_O)_{BD}/\rho_O$ and γ_g is the specific heat ratio of the pressurizing

gas. Thrust coefficient C_F can be evaluated as:

$$C_F = 0.98 \left\{ \sqrt{\frac{2\gamma^2}{\gamma-1}\left(\frac{2}{\gamma+1}\right)^{\frac{\gamma+1}{\gamma-1}}\left[1-\left(\frac{p_e}{p_c}\right)^{\frac{\gamma-1}{\gamma}}\right]} + E\frac{p_e}{p_c} \right\} - E\frac{p_0}{p_c} \tag{11}$$

where a 0.98 correction factor is introduced to modify the vacuum thrust coefficient of a 1-D isentropic expansion to the exit pressure p_e with constant heat ratio γ (Sutton and Biblarz 2001). The term related to the atmospheric pressure p_0 is always small since the third stage always flies at high altitude. Mass flow rate at ignition (i.e. at t=0) can be found as:

$$(\dot{m}_p)_i = (1+\alpha_i)(\dot{m}_F)_i = \frac{1+\alpha_i}{\alpha_i}(\dot{m}_O)_i \tag{12}$$

Initial throat area $(A_{th})_i$ and initial port area $\left(A_p\right)_i$ are then determined:

$$(A_{th})_i = \frac{(\dot{m}_p)_i}{(p_c)_i c_i^*} \;\; ; \qquad (A_p)_i = \frac{(A_{th})_i}{J} \tag{13}$$

where the initial throat area to port area ratio J is set equal to 0.5. Nozzle throat erosion is here considered. The authors use Bartz's method (Ellis 1975; Casalino et al. 2014) to model the dependence of the rate of throat erosion $\dot{s}$ on throat radius R_{th} and chamber pressure p_c:

$$\dot{s} = \dot{s}_{ref}\left(\frac{p_c}{p_{c,ref}}\right)^{0.8}\left(\frac{R_{th,ref}}{R_{th}}\right)^{0.2} \tag{14}$$

R_{th} and E values are computed by integrating Eq. 14. The authors adopt $\dot{s}_{ref} = 0.1$ mm/s obtained from Computational Fluid Dynamics (CFD) analysis on the ablation of a carbon/carbon nozzle for LOX/wax HREs (Bianchi and Nasuti 2013). Our model does not consider erosion along the nozzle, thus obtaining a greater reduction of E and a conservative solution. The authors do not take into account eroded mass, either for thrust augmentation or for rocket mass reduction.

Trajectory Optimization

Once engine design parameters have been defined, the orbit insertion trajectory is optimized by means of an indirect procedure, aiming to maximize the insertion orbit (Casalino et al. 1999; Casalino and Pastrone 2013). The authors consider a point mass rocket for the trajectory optimization. The derivative of position $\boldsymbol{r}$ (radius, latitude and longitude), velocity $\boldsymbol{v}$ (radial, eastward and northward components) and rocket mass M are provided by state equations. In a vectorial form one has:

$$\frac{\mathrm{d}\boldsymbol{r}}{\mathrm{d}t} = \boldsymbol{v} \qquad \frac{\mathrm{d}\boldsymbol{v}}{\mathrm{d}t} = \boldsymbol{g} + \frac{\boldsymbol{F} - \boldsymbol{D}}{m} \qquad \frac{\mathrm{d}M}{\mathrm{d}t} = -\frac{|\boldsymbol{F}|}{c^* C_F} \tag{15}$$

The authors assume an inverse-square gravity field:

$$\boldsymbol{g} = -\frac{GM_\oplus}{||\boldsymbol{r}^3||}\boldsymbol{r} \tag{16}$$

where G is the gravitational constant and $M_\oplus$ is Earth mass. Density and pressure evaluation are computed by means of an interpolation of the standard atmosphere as a function of the rocket altitude. The authors choose to write equations of motion in a non-dimensional form to improve the integration numerical accuracy. Indirect optimization procedure details are here only summarized and can be found in the references (Casalino and Pastrone 2005a). An adjoint variable is associated to each equation; Euler-Lagrange equations, algebraic equations that determine the control variables (i.e., the thrust direction), and the boundary conditions for optimality (which also implicitly define the engine switching times) are provided by the theory of optimal control. A procedure based on Newton's method is used to solve the multi-point boundary value problem which arises. Details can be found in the references (Colasurdo and Pastrone 1994). Tentative values are initially chosen for the problem unknowns and progressively modified to fulfill the boundary conditions. The time lengths of each phase, the initial values of five adjoint variables (the variable corresponding to longitude is null, the one corresponding to the mass is fixed at one, as the problem is homogeneous in the adjoint variables, which can therefore be arbitrarily scaled) are the unknown parameters. Moreover, the overall oxidizer mass and the grain radius are additional unknowns.

Constraints (dynamic pressure, heat flux, acceleration) are not explicitly imposed during the trajectory optimization but are checked "a posteriori". However a constraint that forces horizontal flight at the end of the first burn is added to prevent the rocket from reentering the lower layers of the atmosphere (where the heat flux would become larger). An additional unknown (the adjoint variable corresponding to the horizontal velocity component has a free discontinuity at the end of the first burn) is introduced in the trajectory optimization procedure.

In the present case, the authors consider a hybrid rocket engine suitable for the replacement of third (solid) and fourth (liquid) stage of the Vega launcher (Isakowitz et al. 2004). First and second stage performance and exhausted masses are given, and the conditions at the ignition of the third stage, consistent with a launch from Kourou, are assigned: altitude $h = 86.88$ km, latitude $\phi = 9.11°$, velocity components in the radial, northward and eastward directions $u_r = 0.142$ km/s, $v_n = 0.230$ km/s, $w_e = 4.146$ km/s, respectively, total mass 14,522 kg and fairing mass 540 kg (Casalino and Pastrone 2016). Target final orbit is specified by assigning altitude, eccentricity and inclination (700 km, zero and 90 deg. respectively). The longitude of the ascending node is left free and the fairing is assumed to be jettisoned during the first burn, when the free molecular heat flux reaches 1135 $\mathrm{W/m^2}$.

Robust Design Model

Robust optimization problem can be formally cast as (Park et al. 2006):

$$\begin{aligned} &\text{find} && \boldsymbol{b} \in \mathbb{R}^n \\ &\text{to maximize} && \Phi_{avg}\left(\boldsymbol{b}, \boldsymbol{p}\right) \\ &\text{subject to} && g_j\left(\boldsymbol{b}, \boldsymbol{p} + \boldsymbol{z}^p\right) \leqslant 0, j = 1, ..., r \\ &\text{and to} && \boldsymbol{b}_L \leqslant \boldsymbol{b} \leqslant \boldsymbol{b}_U \end{aligned} \tag{17}$$

where $\boldsymbol{b}$ is the design variables vector, $\boldsymbol{p}$ is the uncertain variables vector, z^p is the noise vector of $\boldsymbol{p}$, g_j is the j-th inequality constraint, $\boldsymbol{b}_L$ and $\boldsymbol{b}_U$ are the lower and upper boundary of the design variables, respectively. In the present approach the initial mass of the upper-stage is given at

ignition, and the payload weight is determined once the propulsion system is defined. Combustion chamber, nozzle, tanks, rocket casing and propellant sliver masses are evaluated by means of suitable assumptions and approximations, whereas feed systems masses are neglected. Details about propulsion system mass evaluation can be found in the references and are here only summarized (Casalino and Pastrone 2010). A 6 mm insulating liner, with a density equal to solid fuel one, and aluminum alloy cylindrical wall are used in the combustion chamber. Aluminum cylindrical oxidizer tank diameter is fixed at 1.9 m, equal to the diameter of Vega's third stage, and the pressurizing gas is contained in a spherical aluminum tank. The wall thickness of tanks and combustion chamber are determined to withstand internal pressure during engine operation, assuming a 1.25 safety factor. In addition, a 1-mm-thick cylindrical aluminum casing encapsulates the HRE. A 45 deg convergent and a 20 deg divergent nozzle, with an ablative layer, is considered. The hydraulic resistance Z is evaluated in order to have $p_t/p_c = 2.5$ at ignition in nominal condition, and six parameters are required to define the propulsion system according to the proposed model. The chosen engine design parameters are: the grain outer radius R_g, the web thickness w, the fuel grain length L_b, the final exhausted oxidizer mass $(m_O)_f$, the exhausted oxidizer mass at the beginning of the BD phase $(m_O)_{BD}$ and the nozzle area ratio E_i. Therefore $\boldsymbol{b} = \left[R_g, w, L_b, (m_O)_f, (m_O)_{BD}, E_i\right]$. Upper and lower boundary of the design variables are shown in Table 1. The choice of lower and upper boundaries for the engine design parameters is done according to requirements relative to the present application (e.g. $2R_g$ lower than outer Vega diameter) and on the basis of user knowledge and past experience (i.e. reduce the range to improve computational speed, without allowing the optimal solution to be on the edges of or outside the design space). Uncertain parameters are the regression rate coefficients a and n, i.e. $\boldsymbol{p} = [a, n]$. The authors take into account uncertainties assigning three different levels for each uncertain variables: $a_i \cdot 10^5 = 9, 9.1, 9.2\,\mathrm{m^{2n+1}s^{n-1}kg^{-n}}$ for $i = 1, 2, 3$, respectively, and $n_j = 0.68, 0.69, 0.7$ for $j = 1, 2, 3$, respectively. The altitude of the attained orbit h_{ij} is evaluated for each of the nine possible couples a_i, n_j. Since two objectives are relevant (i.e. payload μ and altitude h) the authors adopt an ϵ-constraint approach (Haimes et al. 1971) to find the Pareto front of robust solutions. Only average performance is considered here. The average

constraint violation $\Delta_{avg} = \sum_{ij} p_i p_j \max_{ij}(0, h^* - h_{ij})$ is considered. A binomial distribution is assumed giving $p_1 = p_3 = 0.25$ and $p_2 = 0.5$. The average altitude is then $h_{avg} = h^* - \Delta_{avg}$ and the objective function can be computed as:

$$\Phi_{avg} = \mu - k \max(0, \epsilon - h_{avg}) \tag{18}$$

The authors select $k = 20\,\mathrm{kg/km}$ to force the average altitude at ϵ. Only the case $\epsilon = h^* = 700\,\mathrm{km}$ (that is the most demanding in terms of robustness) is here considered.

Hence, design parameters and uncertain parameters, alongside with optimal ascent trajectory, that is optimized by an indirect procedure, determine the value of the robust performance index. The research of the optimal robust design (i.e. the optimal choice of the design parameters of $\boldsymbol{b}$ that maximizes the value of Φ_{avg} despite the presence of uncertainties in $\boldsymbol{p}$) is then performed by means of one of the procedures described in the following section.

ROBUST OPTIMIZATION PROCEDURES

Evolutionary Algorithms: GA and PSO

Two previously developed procedures, namely a GA and a PSO, are used as reference. GA and PSO are both optimization procedures belonging to the class of Evolutionary Algorithms (EAs), that look for an optimal solution in a prescribed search space. GAs apply the biological principle of survival of the fittest in a population of potential solutions called individuals. Basic steps of GAs are shown in Fig. 1. After proper initialization of population, a selection is performed. Then individuals are bred together using operators (such as crossover and mutation) borrowed from natural genetics. The process is iterated and makes the population evolve generation by generation and individuals, which are better suited for the environment, are found (Goldberg 1997; Goldberg and Deb 1991).

PSO is a stochastic optimization technique. It is inspired by the social behavior showed by flock of birds and school of fishes (Kennedy and Eberhart 1995; Eberhart and Kennedy 1995). Unlike GA, PSO has no operators that drive the search. Solutions, here called particles, fly through the

problem space by following the optimum particle (i.e. the alpha-member of the flock or school). The motion of each particle is driven by cognitive and social acceleration and their position and speed are updated at each iteration. Basic steps of PSO are shown in Fig. 2. In most cases PSO tends to converge to global optimal solutions quicker than GA due to its unique information-sharing mechanism (Sentinella and Casalino 2009).

In the present article the maximum number of objective function evaluation is fixed ($N_{FE,max} = 4000$) for all the algorithms. EAs settings are presented in Table 2 and Table 3 for GA and PSO respectively. Additional details about GA and PSO implementation and tuning can be found in the references (Sentinella and Casalino 2009; Sentinella 2008).

Hybrid Algorithm

The first new procedure is a Hybrid algorithm (HA). Hybrid Algorithms combine EAs with some kind of Local Search Operators (LSOs). EAs excel at exploring solutions space but they are pretty slow to converge to the global optimal solution. LSOs, instead, are able to push quickly a solution to its local optimum but can not explore wide areas of the solution space due to their lack of hill-climbing capabilities.

In this work the authors use the aforementioned GA coupled with a brand new crossover operator which implements Taguchi's parameter design method. Parameter design method (also knows as Taguchi's robust design method) was initially developed in the 1980s to improve Japanese mass production and then, it was broadly applied to engineering design problems (Taguchi et al. 2000). The new crossover operator here proposed is an improvement of the one proposed by T.K. Liu and J.H. Chou (Liu and Chou 2004). The basic GA, introduced in the previous subsection, features a starting population of N_I individuals randomly generated, a probability distribution-based crossover (Deb Crossover Operator, DCO), a fixed percentage mutation operators and a tournament selection operator. Elitism principle is used to avoid the loss of information through generations (Sentinella and Casalino 2009). In our new procedure a Taguchi's Crossover Operator (TCO) generates N_{TG} *enhanced offspring* which replace the same number of individuals generated by DCO. The enhancing procedure is based on a 2-level 1-step Taguchi's parameter design method. A pseudo

code for this new TCO can be written as follows:

1. evaluation of the objective function for each of the N_I individuals;
2. ranking of the N_I individuals based on the values of their objective functions;
3. selection of the best $2N_{TG}$ individuals;
4. random coupling of best $2N_{TG}$ individuals (N_{TG} couples, each one made of A and B parents);
5. implementation of Taguchi's 2-level 1-step parameter design method to each couple:
   (a) level 1 assignment to A-parent's parameters and level 2 to B-parent's parameters;
   (b) execution of experimental tests prescribed by suitable orthogonal arrays;
   (c) computation of the mean effect of each level of each parameter;
   (d) selection of the level with the greater mean effect for each parameter;
6. *enhanced offspring* random replacement in the DCO generated population.

In the prescribed tests, uncertain model parameters (i.e. a and n) are taken into account in objective function evaluation, as previously detailed. The new TCO is different from Liu and Chou's crossover operator because they selected randomly the individuals to perform Taguchi's enhancing procedure, while the authors select the better ones after a ranking phase. Basic steps of our HA are shown in Fig. 3: starting random population is initialized and a tournament selection operator is applied. Then the crossover phase starts with the subsequent use of DCO and TCO (see the pseudo code for the details about our TCO). In the end, mass mutation and selection operator are employed and a new generation is created. This process is iterated until the maximum number of function evaluation is reached. In the present article, the authors use $N_I = 40$ in the GA. Tuning procedure of the TCO (see Fig. 4) shows that the selection of a proper value for N_{TG} is crucial. Lower and higher values show poor performance, slowing down the basic GA used in the hybridization process. Intermediate values of N_{TG} seems to be able to boost GA convergence capability without slowing down too much the optimization process. Thus the authors set $N_{TG} = 5$ in our TCO.

The HRE design parameters are 6 and the suitable orthogonal 2-level array is L_8, shown in Figure 5. It requires to execute $n_T = 8$ tests to obtain an *enhanced offspring*. The computational effort for the execution of a single generation of the HA is:

$$N_{FE,G} = N_I + n_T \cdot N_{TG} \tag{19}$$

where $N_{FE,G}$ indicates the number of function evaluation performed for each generation. Note that for the original GA:

$$N_{FE,G} = N_I = 40 \tag{20}$$

Hence, setting $N_{TG} = 5$ in the TCO, the *computational cost per generation* of the HA is exactly twice the GA one. The maximum number of objective function evaluation is fixed ($N_{FE,max} = 4000$) and thus the number of generation is equal to 50 ($N_G = 50$) for the HA. HA settings are summarized in Table 4 for the sake of clarity.

Iterated Local Search

The second new proposed procedure is a meta-heuristic procedure called Iterated Local Search (ILS). Key features of ILS are the use of a specific local search procedure and a solution perturbation criteria (Lourenco et al. 2002). Basic steps of our ILS are shown in Fig. 6 and the relative pseudo-code can be written as follows:

1. find an initial solution s_0 (for instance from previous optimization works on the same problem);
2. apply a local search procedure to s_0 to find the local optimal solution s^*;
3. apply a perturbation criteria to s^* to obtain the perturbed solution $s^{'}$;
4. apply a local search procedure to $s^{'}$ to find the new optimal solution $s^{*'}$;
5. apply an acceptance criterion to the new optimal solution $s^{*'}$ (i.e. $s^{*'}$ performance improved s^* ones);

6. repeat steps 3-5 until a termination condition is reached (i.e. N_{FE} performed equal to $N_{FE,max}$).

ILS is different from the aforementioned EAs because it is not a population-based optimization algorithm. In EAs population is randomly initialized at each generation and thus many objective function evaluation are "wasted" on bad individuals while the algorithm explores the design space. The authors develop ILS with the scope to capitalize on each single objective function evaluation using an efficient local search procedure, since the evaluation of the problem specific objective function is really expensive in terms of computational time. On the other hand, EAs are not influenced by the selection of the initial tentative solution because they do not require it at all. The effectiveness of an optimization procedure strongly depends on the problem to be optimized itself, but both EAs and ILS have promising features. The authors implement ILS in particular to compare its capabilities, in the optimization of our HRE, with EAs. In addition, from an engineering point of view, it is generally better to have more than a single optimization tool available (i.e. PSO and ILS) when a new problem comes out.

In the present work, the authors take advantage of Taguchi's Multi-step 3-level parameter design Method (TMM) as a local search procedure. Moreover, the authors also develop a perturbation criteria that is driven at each iteration by the results of TMM. TMM is based on Taguchi's robust design method (Taguchi et al. 2000; Yao et al. 2011; Park et al. 2006; Lee et al. 1996), whose core idea is that design parameters can be split into two groups: noise factors and control factors. Noise factors are parameters whose values are affected by uncertainties and variations that could be impossible or too costly to avoid. Control factors are, instead, design parameters whose values could be freely chosen by the designers. Taguchi's parameter design method main tools were two orthogonal experimental arrays (called outer and inner arrays) that were used to assign discrete values (called levels) to each factor and perform experimental tests (i.e. objective function evaluation). Experimental tests results were then used to perform an ANalysis Of Means (ANOM) and an ANalysis Of VAriance (ANOVA) of the objective function values. In the end, ANOM and ANOVA prescribed the optimal level for each control factor that gave the best objective function

value and minimized the effect of the noise factors.

In our original TMM this procedure is executed iteratively. Levels are assigned at each step according to an equally spaced experimental grid which discretized the design space. At each step the solution is pushed closer to the local optimal solution by ANOM and ANOVA. When a local optimal solution is reached, ILS kicks in and perturbs that solution according to the last ANOVA. Our idea is that control factors that show a smaller impact on objective function should be perturbed the most and vice versa. This perturbation criteria is used to enhance ILS hill-climbing capabilities and, hopefully, to drive the local search procedure to a global optimal solution. ILS settings are summarized in Table 5. The choice of the perturbation constant K (i.e. the maximum magnitude of the perturbation) is the most critical, as presented in Fig. 7. A small constant (i.e. $K = 10$) leads to poor hill-climbing capabilities while a large constant (i.e. $K = 100$) results in slowing down the algorithm moving the tentative solution too far away from feasible solutions at every restart of the local search procedure. After several tuning runs of the optimization procedure, the authors set $K = 40$. Each control parameter perturbation size depends on the product of the reciprocal of its ANOVA contribution, a random number in the range [0,1] and the perturbation buffer K. In this way the perturbation can span from zero to K discretization steps.

The perturbation buffer B is defined as the number of iteration of the local search procedure, without solution improvement, that the ILS has to wait before the perturbation kicks in. In Fig. 8 optimization runs, for different values of the buffer, are presented. One can notice that the higher is the value of B, the lower results to be the mean performance index. This behavior seems to be caused by searching loops among very similar solutions when the local search procedure reaches a local optimal point. Thus, B is set equal to one to minimize the waste of function evaluation inside these loops. Since the authors deal with 6 control factors with 3 levels each, L_{18} (Figure 9) is used as inner arrays for the TMM. Analogously, since 2 noise factors (i.e. regression rate classical formulation coefficients a, n) with 3 levels each are present, the authors use L_9 (Figure 10) as outer arrays. The factors combinations, prescribed by L_9, have been already taken into account in the objective function formulation as nine a_i, n_j couples used in the evaluation of h_{ij}.

NUMERICAL RESULTS

As described in the previous sections, a two-layer optimization is employed for trajectory and engine design: the indirect trajectory optimization maximizes the final mass given engine geometry, which, in turn, is optimized by means of a robust-based design approach. The authors repeat the optimization process five times using each robust-based procedure. Given $N_{FE,max} = 4000$, the average run on a 3 GHz machine is 15 hours. Note that the final burn of the HRE has a very short duration and a limited influence on the rocket performance. Hence subsequent figures show only the first burn for the sake of simplicity. Table 7 shows a comparison between the best robust solutions and the relative design parameters values found out by each algorithm. Deterministic optimum design and performance is also reported as DET.

Looking at the values of R_g, w and L_b for the optimized robust solutions, one can notice that $\left(\frac{A_{le}}{A_b}\right)_{\%} \approx 10\%$ (exact values are shown in Table 6). Nevertheless, the relative contribution of lateral end decreases from these values down to zero during the engine operation. Moreover the regression rate in the lateral end of the grain is actually smaller than cylindrical burning area one. Thus, the assumption about the negligible extent of the lateral end contribution to combustion, made in our model, results to be valid.

Due to the large value for k in Eq. 18, the average height violation is forced to zero and Φ coincides with the payload for the robust designs. On the other hand, the deterministic design has the largest payload (2280.9 kg) but a large average height violation (171.8 km) too. From an objective function point of view ILS and PSO converge to optimum points characterized by $\Phi_{avg} \approx 2070\,\text{kg}$ while GA and HA provide worse solutions. These results confirm that PSO has better convergence capabilities than GA. Moreover ILS has a similar performance compared to PSO, since its optimum design point is comparable to PSO, and better than GA. However PSO and ILS solutions differ in terms of design parameters: the optimal values of some parameters are close to each other (R_g, w, $(m_O)_f$ and $(m_O)_{BD}$) while others are quite different (L_b and E). This could suggest that PSO and ILS solutions maximize the objective function in different ways: PSO tries to reduce propellant consumption improving propulsion system performance (larger expansion ratio,

shorter grain, higher mixture ratio and I_{SP} as shown in Fig. 11 and Fig. 12), while ILS tries to reduce engine dry mass (smaller expansion ratio and longer grain). Moreover the two optimum solutions (or at least one of them) seems to be only a locally optimal solutions. HA finds an optimum point which is better than the one found by GA, and quite close to the PSO and the ILS ones. Furthermore, one can notice, thanks to Fig. 13, that also the thrust histories are close to each other for PSO, ILS and HA, whereas GA exhibits an higher initial thrust level. Thus, GA performance results to be enhanced by the hybridization process (i.e. the use of TCO instead of standard crossover operators). The payload gain of the robust optimized solutions, with respect to the Vega launcher, is roughly equal to 600 kg. The main sources of performance improvement are a remarkable saving in the dry masses of the upper stages (only one HRE powered stage vs. two upper stages), slightly higher specific impulse and reduced $\Delta \boldsymbol{v}$ losses.

Looking at Table 7, one can notice that initial expansion ratios E_i of optimal solutions are much smaller than conventional ones for liquid-powered upper stages. This optimization strategy is due to the trade-off between the increase in nozzle performance and the reduction of its mass. Complex cooling systems for the nozzle, typical of LREs such as regenerative cooling, cannot be employed in HREs. Therefore, an ablative cooling is considered by the authors, similar to SRMs one, for the present test case. Ablative cooling is a simple and cheap solution (i.e. really suitable for HREs), but the resulting nozzle tends to be heavy and thus smaller expansion area ratios are preferred in the optimization process.

Table 8 summarizes engine performance of the best solutions presented in Table 7. Looking at Fig. 11 one can notice that the mixture ratio shifting is limited, since α varies approximately between 2 and 2.5, whereas in Table 8 chamber pressure p_c roughly varies from $4{\cdot}10^5$ Pa to $10{\cdot}10^5$ Pa, showing a wider range of variation. Thus, in the present case, the effect of mixture ratio shifting and chamber pressure variation on characteristic velocity c^* and specific heat ratio γ is expected to be similar. The authors considered only the effect of α in the optimization process, neglecting chamber pressure one. However, both effects results to be small and thus no further computations of engine performance are required.

Looking at Table 8 one can notice that the maximum chamber pressure $(p_c)_{max}$ is always equal to $10 \cdot 10^5$ Pa for all robust solutions, regardless of the optimization algorithm used. In the Robust Design Model subsection, hydraulic resistance Z is reported to be evaluated to grant $p_t/p_c = 2.5$. The authors adopted a gas-pressurized feed system in the present application, thus the maximum tank pressure is equal to the initial one, that is fixed to $25 \cdot 10^5$ Pa. Hence, the maximum chamber pressure $(p_c)_{max}$ is always equal to $10 \cdot 10^5$ Pa.

Table 9 shows mean and range of variation of the optimal objective function values distribution. One more time, PSO and ILS optimal solutions are close to each other, both in term of mean value and range of variation of the objective function of the optimum points. On the contrary, HA and GA optimum solutions exhibit a greater fluctuation around a worse mean objective function value. Low mean and high range of variation values of HA and GA solutions can be due to the coupling of their lower convergence speed with the common limitation of the number of function evaluation. Figure 14 shows a comparison of the performance index evolution for the best optimization run for each algorithm. From these curves one can notice that PSO, ILS and GA rate of improvement tends to be negligible after $N_{FE} = 3000$ while it is still significant for HA. Hence HA could show a better behavior in longer (in terms of number of function evaluations) optimization runs. In the present article the authors fix the computational effort for all algorithms and therefore they do not examine in depth this aspect of HA.

CONCLUSIONS

An indirect trajectory optimization procedure has been coupled with different robust-based design methods to optimize a hybrid rocket engine. Two new robust-based design approaches based on different principles (i.e. HA and ILS) have been presented and their performance have been compared to those of two previously developed approaches: PSO and GA. The optimization of an upper stage of a Vega-like launcher has been considered. The optimization is performed for a given insertion orbit and lift-off weight. Regression rate uncertainties are taken into account. A linear combination of payload and average altitude has been used as mission specific performance index. The chosen index formulation forces the solution to nullify the spread of the orbit altitude, thus

assuring the required robustness. Performance of the four robust-based approaches are compared using a constant number of function evaluations. Several runs have been carried out for each of the considered procedures.

One of the new procedures, i.e. the Iterated Local Search, is able to converge to optimum designs that have performance as good as the ones identified by the best population-based algorithm present in the comparison, i.e. the PSO. The difference of the payload for the best solutions of ILS and PSO is only 0.5 kg, i.e. about 0,02%. Considering the different runs, the spread of the payload is low. GA shows far worse solutions, both considering payload and results spread. Our comparison clearly shows that GA is not suitable for robust optimization of this kind of problems. The other new procedure, Hybrid Algorithm, is able to enhance GA performance. Nevertheless HA range of variation is remarkably high, pointing out that a better and coupled tuning of the chosen local search operator and basic GA is required to match PSO and ILS performance.

Looking at the values of the design parameters, one can realize that PSO and ILS follow two different optimization strategies, resulting in very similar performance: PSO improves the propulsion system performance whereas ILS reduces engine dry mass. Nevertheless, at least one of the solutions is only a local optimum. An higher number of runs with a larger number of function evaluation should be required to establish the best robust design approach. On the other hand, from an engineering point of view, both the methods can provide a sufficiently robust design with a reasonable computation effort. ILS and PSO belong to two different class of optimizer allowing for a wider solution capability. In the present application, one run involves 4000 evaluations of the performance index and requires about 15 hours on a 3 GHz machine.Note that here uncertainty has been taken into account for only two parameters (i.e. coefficient a and exponent n in the regression rate correlation). If a larger number of uncertain parameters is considered, the computational time required for the optimization process may explode. For this reason, additional approximate approaches could be considered in future works to deal with the excessive computation effort of the coupled robust optimization procedure.

NOTATION

The following symbols are used in this paper:

A_b = burning surface area (m^2);

A_p = port area (m^2);

A_{th} = nozzle throat area (m^2);

a = regression constant (m^{1+2n} kg^{-n} s^{n-1});

B = ILS perturbation buffer;

$\boldsymbol{b}$ = design variables vector;

$\boldsymbol{b}_L$ = lower bound vector;

$\boldsymbol{b}_U$ = upper bound vector;

C_F = thrust coefficient;

c^* = characteristic velocity (m/s);

$\boldsymbol{D}$ = drag vector (N);

D = rocket outer diameter (m);

E = nozzle area-ratio;

$\boldsymbol{F}$ = thrust vector (N);

F = thrust (N);

G = gravitational constant (Nm^2/kg^2);

$\boldsymbol{g}$ = gravity acceleration (m/s^2);

$g_j(\boldsymbol{b})$ = j-th inequality constraint;

h = altitude (km);

h^* = target altitude (km);

I_{SP} = specific impulse (s);

J = initial throat area to port area ratio;

K = ILS perturbation constant;

k = linear combination constant (kg/km);

L = overall engine length (m);

L_b = fuel grain length (m);

M = rocket mass (kg);

$M_\oplus$ = Earth mass (kg);

m = mass (kg);

N = number;

n = mass-flux exponent;

P = burning perimeter (m);

$\boldsymbol{p}$ = uncertain variables vector;

p = pressure (Pa);

R_g = grain outer radius (m);

R_i = grain initial inner radius (m);

R_{th} = throat radius (m);

$\boldsymbol{r}$ = position vector (m);

s = eroded distance (mm);

t = time (s);

u_r = velocity component in the radial direction (km/s);

V = volume (m^3);

$\left(V_g\right)_i$ = initial ullage volume (m^3);

v_n = velocity component in the northward direction (km/s);

$\boldsymbol{v}$ = velocity vector (m/s);

w = web thickness (m);

w_e = veocity component in the eastward direction (km/s);

y = burning distance (m);

Z = hydraulic resistance (1/(kg m));

$\boldsymbol{z}^p$ = noise vector of $\boldsymbol{p}$

α = mixture ratio;

γ = specific heat ratio;

Δ = altitude violation (m);

ϵ = multi-objective constraint (km);

$\mathbf{\Lambda}$ = steps lengths;

μ = payload (kg);

ρ = density (kg/m^3);

Φ = objective function (kg);

ϕ = latitude (deg);

Superscripts

$\dot{}$ = time derivative;

Subscripts

0 = ambient;

1 = combustion chamber at head-end;

a = auxiliary gas;

avg = average;

BD = beginning of blowdown phase;

c = combustion chamber at nozzle entrance;

e = nozzle exit;

F = fuel;

FE = objective function evaluations;

G = generations;

g = pressurizing gas;

I = individuals;

i = initial value;

le = lateral end;

max = maximum;

min = minimum;

O = oxidizer;

p = overall propellant (oxidizer + fuel);

ref = reference;

stp = steps;

TG = Taguchi enhanced offspring;

t = oxidizer propellant tank;

vac = vacuum;

REFERENCES

Barrere, M., Jaumotte, A., De Veubeke, B. F., Vandenkerckhove, J., (1960). *Rocket Propulsion*, Elsevier Publishing Company, 251-256, Amsterdam, NL.

Bianchi, D., and Nasuti, F., (2013). "Numerical Analysis of Nozzle Material Thermochemical Erosion in Hybrid Rocket Engines", *Journal of Propulsion and Power*, 29(3), 547-558.

Box, G. E. P., and Fung, C., (1993). "Is Your Robust Design Procedure Robust?", *Quality Engineering*, 6(3),503-514.

Brown, C. D., (1992). "Spacecraft Propulsion", *AIAA Education Series*, p. 82, Washington, DC.

Cantwell, B. J., Karabeyoglu, M. A., and Altman, D., (2010). "Recent Advances in Hybrid Propulsion", *International Journal of Energetic Materials and Chemical Propulsion*, 305-326.

Casalino, L., and Pastrone, D., (2008). ''Optimal design of hybrid rocket motors for microgravity platform", *Journal of Propulsion and Power*, 24(3), 491-498.

Casalino, L., and Pastrone, D., (2012). "Optimization of Hybrid Sounding Rockets for Hypersonic Testing", *Journal of Propulsion and Power*, 28(2), 405-411.

Casalino, L., and Pastrone, D., (2015). ''A Straightforward Approach for Robust Design of Hybrid Rocket Engine Upper Stage", *51st AIAA/SAE/ASEE Joint Propulsion Conference*, AIAA, Orlando, FL.

Casalino, L., Letizia, F., and Pastrone, D., (2014). "Optimization of Hybrid Upper-Stage Motor with Coupled Evolutionary/Indirect Procedure", *Journal of Propulsion and Power*, 30(5).

Casalino, L., and Pastrone, D., (2016). "Optimal Robust Design of Hybrid Rocket Engines", *Springer Optimization and Its Applications*, Springer, 269-285.

522 Casalino, L., and Pastrone, D., (2005a). ”Optimal Design and Control of Hybrid Rockets for Access
523 to Space”, *41st AIAA/ASME/SAE/ASEE Joint Propulsion Conference & Exhibit*, AIAA, Tucson,
524 AZ.
525 Casalino, L., and Pastrone, D., (2010). ”Optimal Design of Hybrid Rocket Motors for Launchers
526 Upper Stages”, *Journal of Propulsion and Power*, 26(3), 421-427.
527 Casalino, L., and Pastrone, D., (2013). ”Integrated Design-Trajectory Optimization for Hybrid
528 Rocket Motors”, *Modeling and Optimization in Space Engineering*, Springer, 343-363.
529 Casalino, L., Colasurdo, G., and Pastrone, D., (1999). ”Optimal Low-Thrust Escape Trajectories
530 Using Gravity Assist”, *Journal of Guidance, Control, and Dynamics*.
531 Casalino, L., and Pastrone, D., (2005b). ”Oxidizer Control and Optimal Design of Hybrid Rockets
532 for Small Satellites”, *Journal of Propulsion and Power*.
533 Colasurdo, G., and Pastrone, D., (1994). " Indirect Optimization Method for Impulsive Transfer",
534 *Astrodynamics Conference*, Scottsdale,AZ.
535 Dornheim, M. A., (2004). ”Reaching 100 km”, *Aviation Week & Space Technology*, 161(6), 45-46.
536 Eberhart, R., and Kennedy, J., (1995). ”A New Optimizer Using Particle Swarm Theory”, *Sixth*
537 *International Symposium on Micro Machine and Human Science*, Institute of Electrical and
538 Electronics Engineers, 39-43.
539 Ellis, R. A., (1975). *Solid Rocket Motor Nozzles-NASA Space Vehicle Design Criteria (Chemical*
540 *Propulsion)*, NASA, Cleveland, OH.
541 Goldberg, D., (1997). *Genetic Algorithms in Engineering Design*, Wiley, New York, NY.
542 Goldberg, D., and Deb, K., (1991). ”A Comparison of Selection Schemes Used in Genetic Algo-
543 rithms”, *Foundations of Genetic Algorithms*, 1, 450-457.
544 Haimes, Y., Lasdon, L., and Wismer, D., (1971). ”On a Bicriterion Formulation of the Problems
545 of Integrated System Identification and System Optimization”, *IEEE Transactions on Systems,*
546 *Man, and Cybernetics*, 296-297.
547 Isakowitz, S. J., Hopkins, J. A., and Hopkins, J. A., Jr., (2004). *International Reference Guide to*
548 *Space Launch Systems*, 4th ed., AIAA, 517-524, Portland, OR.

549 Jens, E., Karp, A. C., Nakazono, B., Eldred, D. B., DeVost, M. E., and Vaughan, D., (2016),
550 "Design of a Hybrid CubeSat Orbit Insertion Motor", *52nd AIAA/SAE/ASEE Joint Propulsion*
551 *Conference*, AIAA, Salt Lake City, UT.
552 Karabeyoglu, M. A., Altman, D., and Cantwell, B. J., (2002). "Combustion of Liquefying Hybrid
553 Propellants: Part 1, General Theory", *Journal of Propulsion and Power*, 18(3), 610-620.
554 Karp, A. C., Nakazono, B., Manrique, J. B., Shotwell, R., Vaughan, D., and Story, G.T., (2016).
555 "A Hybrid Mars Ascent Vehicle Concept for Low Temperature Storage and Operation", *52nd*
556 *AIAA/SAE/ASEE Joint Propulsion Conference*, AIAA, Salt Lake City, UT.
557 Kennedy, J., and Eberhart, R., (1995). "Particle Swarm Optimization", *Proceedings of the IEEE*
558 *International Conference on Neural Networks, Institute of Electrical and Electronics Engineers*,
559 1942-1948.
560 Lee, K. H., Eom, I. S., Park, G. J., and Lee, W. I., (1996). "Robust Design for Unconstrained
561 Optimization Problems Using the Taguchi Method", *AIAA Journal*, 34(5), 1059-1063.
562 Liu, T. K., Chou, J. H., (2004). "Hybrid Taguchi-Genetic Algorithm for Global Numerical Opti-
563 mization", *IEEE Transactions on Evolutionary Computation*.
564 Lourenco, H. R., Martin, O., and Stützle, T., (2002). *Handbook of Metaheuristics*, Kluwer Academic
565 Publishers, 321-345, Dordrecht, NL.
566 Mc Bride, B.J., Reno, M.A., and Gordon, S., (1994). *CET93 and CETPC: an Interim Updated*
567 *Version of the NASA Lewis Computer Program for Calculating Complex Chemical Equilibria*
568 *with Applications*, NASA, Cleveland, OH.
569 Park, G. J., Lee, T. H., Lee, K. H., and Hwang, K. H., (2006). "Robust Design: An Overview",
570 *AIAA Journal*, 44(1), 181-191.
571 Pastrone, D., (2012), "Approaches to Low Fuel Regression Rate in Hybrid Rocket Engines",
572 *International Journal of Aerospace Engineering*, 2012.
573 Sentinella, M. R., and Casalino, L., (2009). "Hybrid Evolutionary Algorithm for the Optimization
574 of Interplanetary Trajectories", *Journal of Spacecraft and Rockets*, 46(2).
575 Sentinella, M. R., (2008). "Development of New Procedures and Hybrid Algorithms for

576 Space Trajectories Optimisation", Ph.D. Dissertation, Dipartimento di ingegneria meccanica
577 e aerospaziale, Politecnico di Torino, Turin, IT.
578 Suh, N. P., (2001). *Axiomatic Design: Advances and Applications*, Oxford University Press, New
579 York, NY.
580 Sutton, G.P., Biblarz, O., (2001). *Rocket Propulsion Elements*, 7th ed., Wiley, New York, NY.
581 Taguchi, G., Chowdhury, S., and Taguchi, S., (2000). *Robust Engineering*, McGraw–Hill, New
582 York, NY.
583 Yao, W., Chen, X., Luo, W., Van Tooren, M., and Guo, J., (2011). "Review of Uncertainty Based
584 Multidisciplinary Design Optimization Methods for Aerospace Vehicle", *Progress in Aerospace*
585 *Sciences*.

List of Tables

TABLE 1. Design parameters ranges.

Boundary	R_g	w	L_b	$(m_O)_f$	$(m_O)_{BD}$	E_i
	m	m	m	kg	kg	-
$\boldsymbol{b}_L$	0.55	0.25	4.3	6971	3195	15
$\boldsymbol{b}_U$	0.60	0.35	4.5	7697	3631	20

TABLE 2. GA settings.

Setting	Value
Number of generations, N_G	100
Number of individuals, N_I	40
Dimension of individuals	6
Ranges of individuals	$\boldsymbol{b}_U - \boldsymbol{b}_L$
Selection operator	Tournament
Selection pressure	2.0
Crossover operator	Deb Crossover
Mass mutation parameter	98%

TABLE 3. PSO settings.

Setting	Value
Number of generations, N_G	100
Number of particles, N_I	40
Dimension of particles	6
Ranges of particles	$\boldsymbol{b}_U - \boldsymbol{b}_L$
PSO method	1-trelea type 1
Cognitive acceleration, $C1$	2.0
Social acceleration, $C2$	2.0
Check population method	Saturation
End velocity weight	0.4
Linear varying factor	0.2
Maximum velocity, V_{max}	$0.25(\boldsymbol{b}_U - \boldsymbol{b}_L)$
Mass mutation parameter	98%

TABLE 4. HA settings.

Setting	Value
Number of generations, N_G	50
Number of individuals, N_I	40
Number of *enhanced offspring*, N_{TG}	5
Dimension of individuals	6
Ranges of individuals	$\boldsymbol{b}_U - \boldsymbol{b}_L$
Selection operator	Tournament
Selection pressure	2.0
Crossover operator	DCO + TCO
Mass mutation parameter	98%

TABLE 5. ILS settings.

Setting	Value
Discretization steps, N_{stp}	100
Perturbation constant, K	40
Perturbation buffer, B	1
Dimension of solutions	6
Ranges of solutions	$\boldsymbol{b}_U - \boldsymbol{b}_L$
Steps length, $\boldsymbol{\Lambda}$	$(\boldsymbol{b}_U - \boldsymbol{b}_L)/N_{stp}$

TABLE 6. Lateral end contributions.

Solutions	$\left(\frac{A_{Le}}{A_b}\right)_{\%}$ -
DET	9.01%
PSO	10.08%
ILS	9.82%
HA	10.06%
GA	9.63%

TABLE 7. DET, PSO, ILS, HA e GA results comparison.

Solutions	R_g	w	L_b	$(m_O)_f$	$(m_O)_{BD}$	E_i	μ	Δ_{avg}	Φ_{avg}
	m	m	m	kg	kg	-	kg	km	kg
DET	0.585	0.276	4.430	7350	3269	15.00	2280.9	171.8	-1134.9
PSO	0.591	0.294	4.360	7403	3195	17.32	2069.8	0.0	2069.8
ILS	0.591	0.293	4.452	7372	3212	15.70	2069.3	0.0	2069.3
HA	0.589	0.295	4.404	7369	3318	18.18	2062.2	0.0	2062.2
GA	0.587	0.290	4.482	7391	3598	16.01	2049.8	0.0	2049.8

TABLE 8. PSO, ILS, HA e GA engine performance comparison.

Solutions	$(F_{vac})_{min}$	$(F_{vac})_{max}$	$(I_{SP})_{avg}$	$\dot{y}_{min}$	$\dot{y}_{max}$	α_{avg}	$(p_c)_{min}$	$(p_c)_{max}$
	kN	kN	s	m/s	m/s	-	Pa	Pa
PSO	104.8	242.6	297.9	$7.70 \cdot 10^{-4}$	$3.53 \cdot 10^{-3}$	2.16	$3.84 \cdot 10^{5}$	$10.00 \cdot 10^{5}$
ILS	105.5	241.8	296.3	$7.80 \cdot 10^{-4}$	$3.52 \cdot 10^{-3}$	2.12	$3.88 \cdot 10^{5}$	$10.00 \cdot 10^{5}$
HA	107.5	237.7	298.7	$7.90 \cdot 10^{-4}$	$3.51 \cdot 10^{-3}$	2.13	$4.00 \cdot 10^{5}$	$10.00 \cdot 10^{5}$
GA	111.6	254.6	296.7	$8.50 \cdot 10^{-4}$	$3.51 \cdot 10^{-3}$	2.14	$4.35 \cdot 10^{5}$	$10.00 \cdot 10^{5}$

TABLE 9. PSO, ILS, HA e GA mean results and ranges.

Solutions	Mean	Range
	kg	kg
PSO	2065.74	5.84
ILS	2065.81	6.69
HA	2047.17	26.89
GA	2036.08	22.07

List of Figures

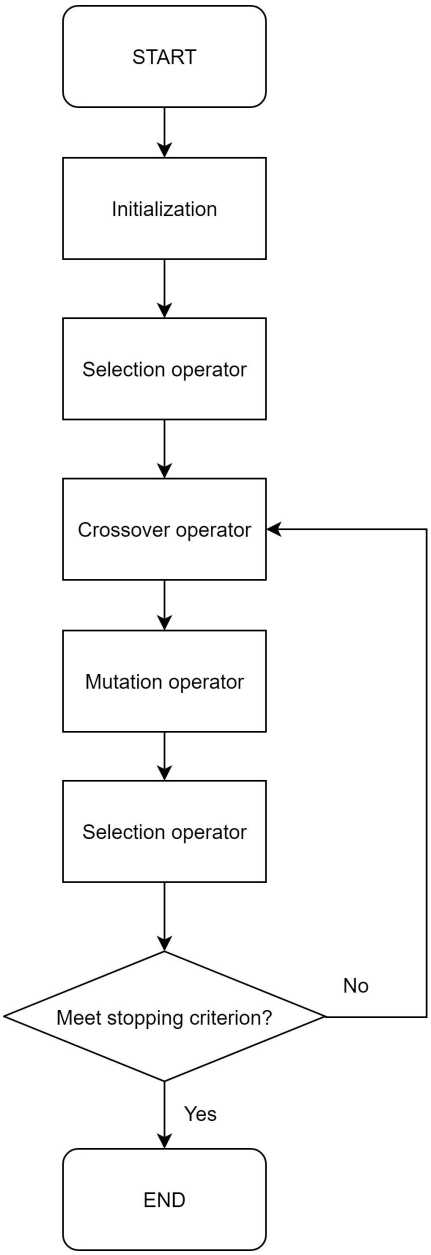

FIG. 1. GA: flow chart.

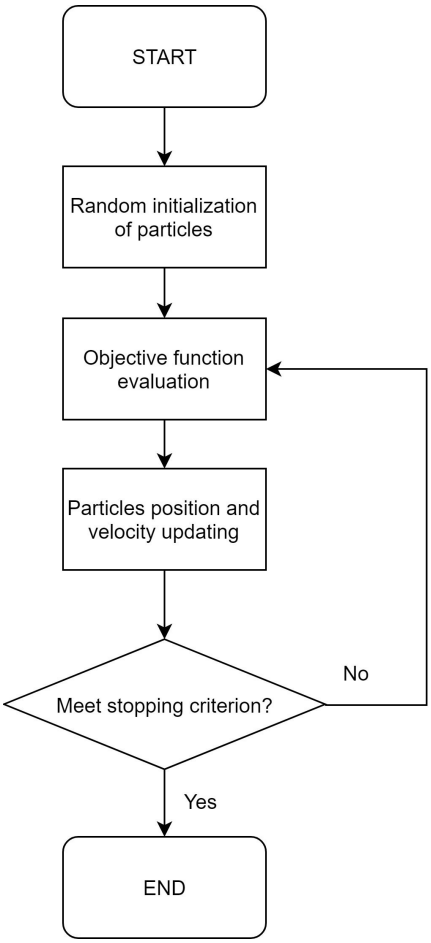

FIG. 2. PSO: flow chart.

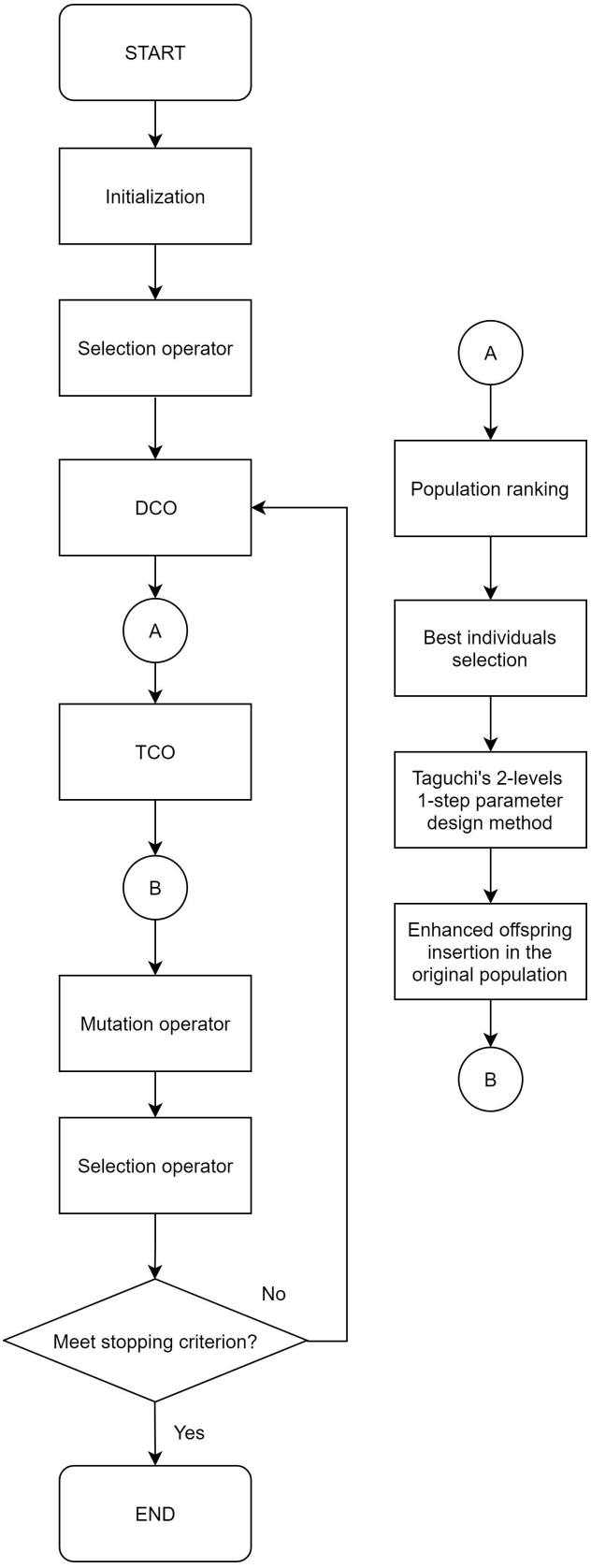

FIG. 3. HA: flow chart.

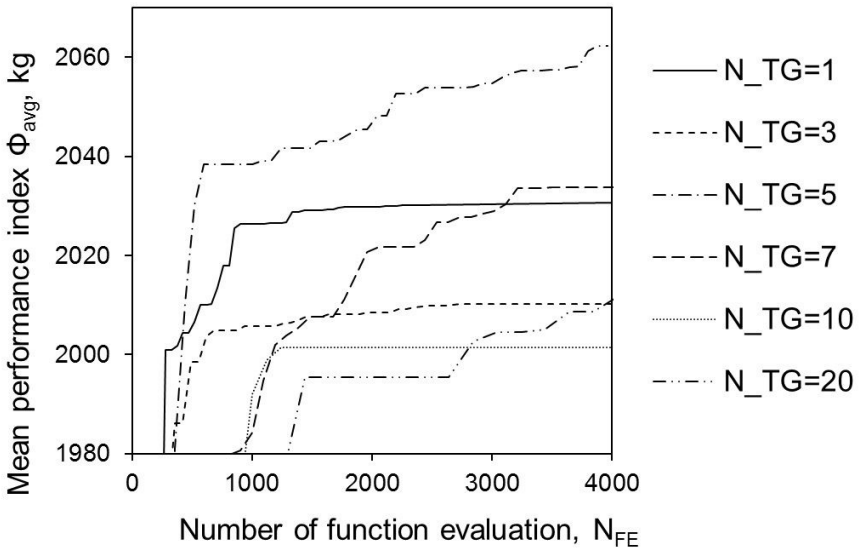

FIG. 4. Tuning of N_{TG}.

1	1	1	1	1	1
1	1	1	2	2	2
1	2	2	1	2	2
1	2	2	2	1	1
2	1	2	2	1	2
2	1	2	1	2	1
2	2	1	2	2	1
2	2	1	1	1	2

FIG. 5. L_8 **orthogonal arrays.**

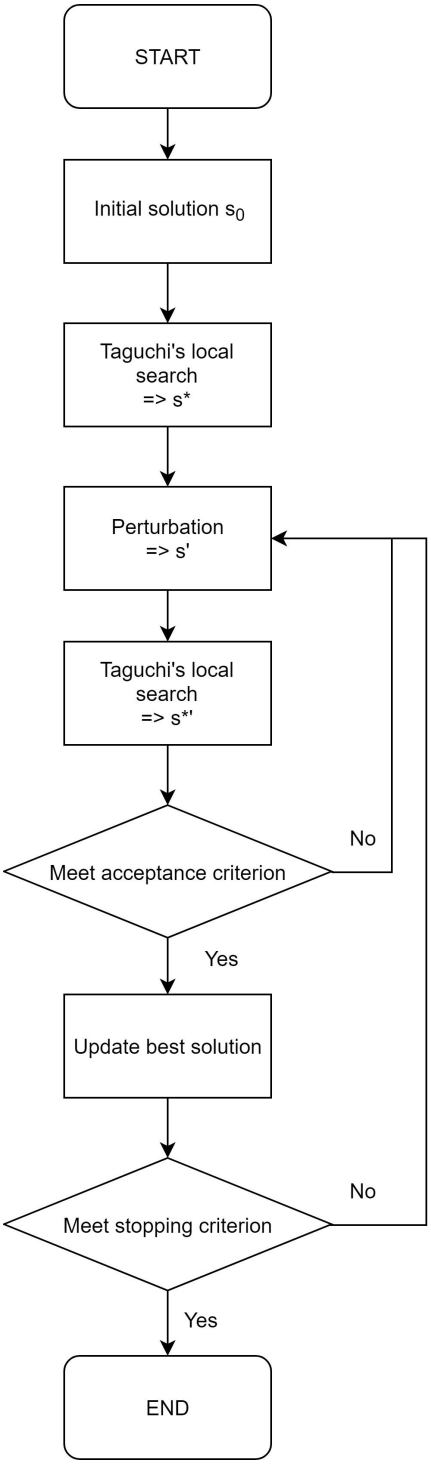

FIG. 6. ILS: flow chart.

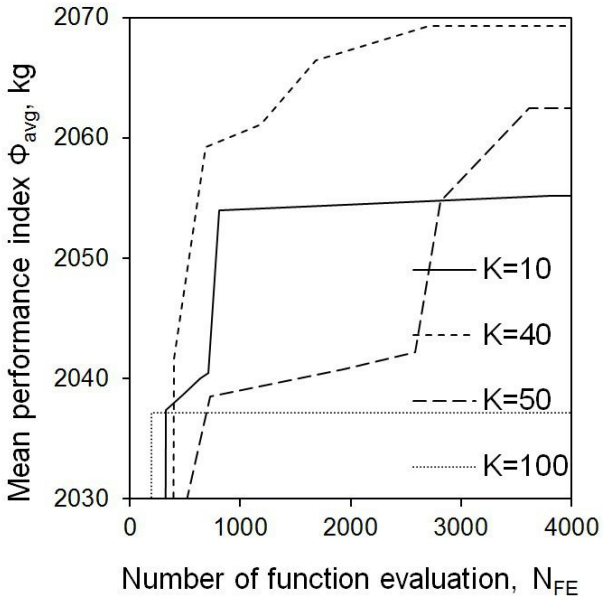

FIG. 7. Tuning of perturbation constant K (with $B = 1$).

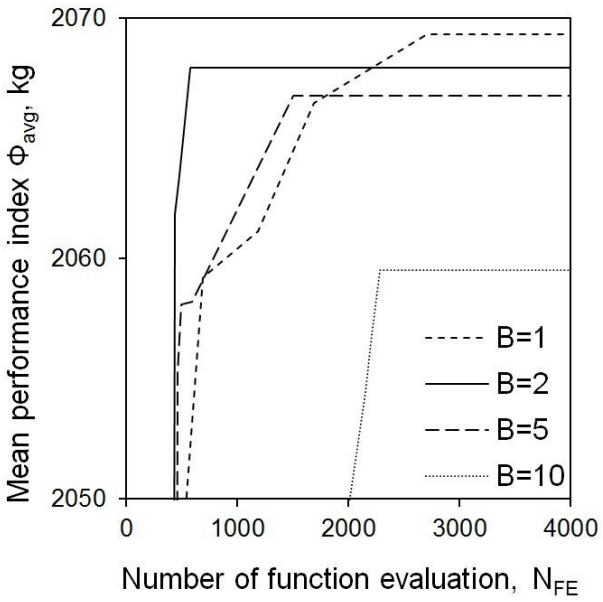

FIG. 8. Tuning of perturbation buffer B (with $K = 40$).

1	1	1	1	1	1
1	2	2	2	2	2
1	3	3	3	3	3
2	1	1	2	3	3
2	2	2	3	1	1
2	3	3	1	2	2
3	1	2	3	2	3
3	2	3	1	3	1
3	3	1	2	1	2
1	1	3	2	2	1
1	2	1	3	3	2
1	3	2	1	1	3
2	1	2	1	3	2
2	2	3	2	1	3
2	3	1	3	2	1
3	1	3	3	1	2
3	2	1	1	2	3
3	3	2	2	3	1

FIG. 9. L_{18} **orthogonal arrays.**

1	1
1	2
1	3
2	1
2	2
2	3
3	1
3	2
3	3

FIG. 10. L_9 **orthogonal arrays.**

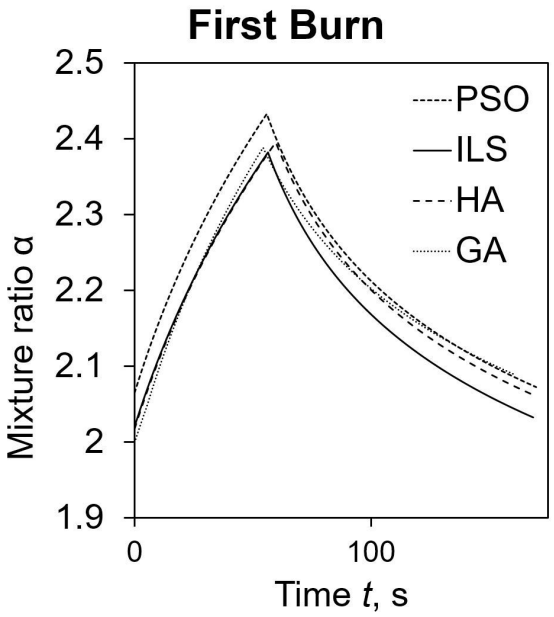

FIG. 11. Mixture ratio history.

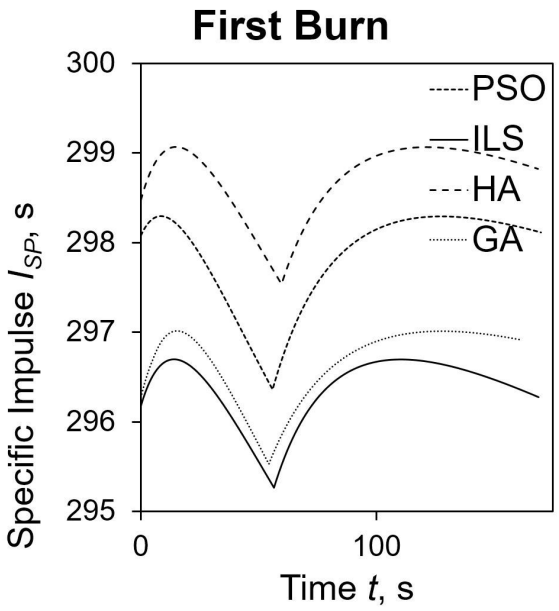

FIG. 12. I_{SP} **history.**

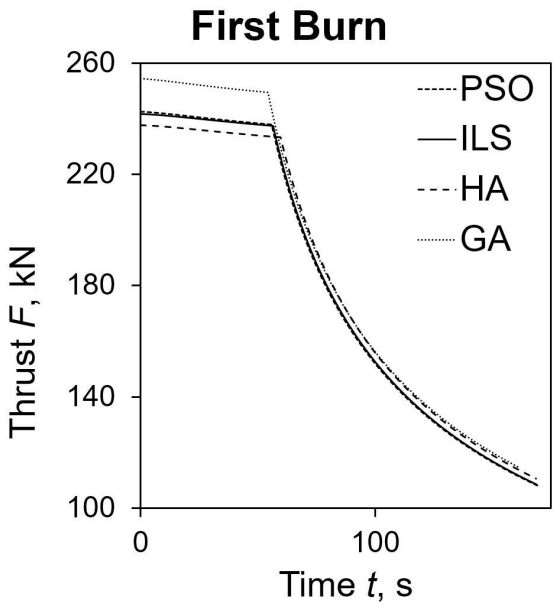

FIG. 13. Thrust history.

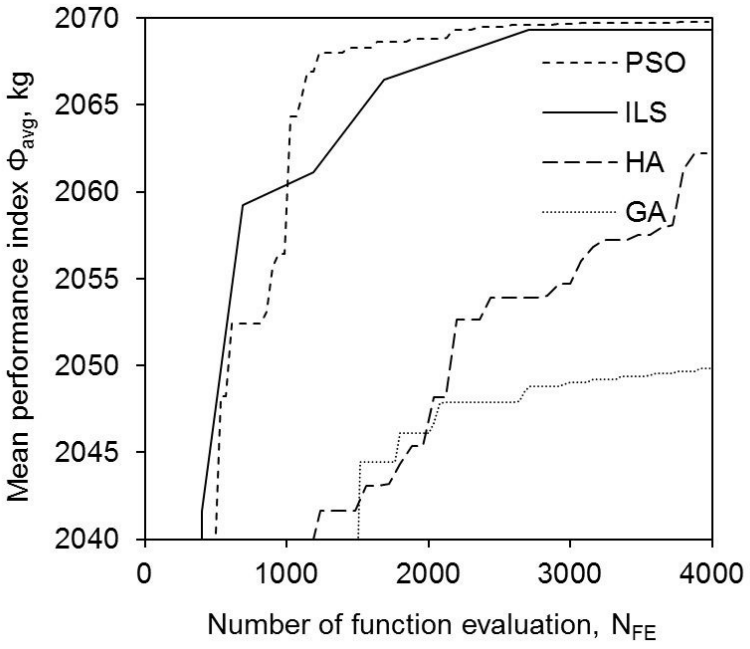

FIG. 14. Mean performance index Φ_{avg} vs. number of function evaluation N_{FE}.